Biosensors and Bioelectronics 133 (2019) 141–146

Contents lists available at ScienceDirect

Biosensors and Bioelectronics

journal homepage: www.elsevier.com/locate/bios

Stepping gating of ion channels on nanoelectrode via DNA hybridization for label-free DNA detection

Haipei Zhao[a,c], Dekai Ye[c], Xiuhai Mao[b], Fan Li[b], Jiaqiang Xu[a,*], Min Li[b,*], Xiaolei Zuo[b]

[a] NEST Lab, Department of Chemistry, College of Sciences, Shanghai University, Shanghai 200444, China
[b] Institute of Molecular Medicine, Renji Hospital, School of Medicine, Shanghai Jiao Tong University, Shanghai 200127, China
[c] Division of Physical Biology & Bioimaging Center, Shanghai Synchrotron Radiation Facility, CAS Key Laboratory of Interfacial Physics and Technology, Shanghai Institute of Applied Physics, Chinese Academy of Sciences, Shanghai 201800, China

ARTICLE INFO

Keywords:
Stepping gating
Ion channel
Nanoelectrode
Electrochemical
Label-free DNA detection

ABSTRACT

Natural ion channels on cell membrane can gate the transport of ions and molecules by the conformational alteration of transmembrane proteins to regulate the normal physiological activities of cells. Inspired by the similarity of the conformation change under specific stimuli, here we introduce an ion channel gating model on a single nanoelectrode by anchoring DNA-gated switches on the very nanotip of gold nanoelectrode to mimic the response-to-stimulus behaviors of ion channels on bio-membranes. The surface-tethered DNA ion channels can be switched on by the Watson-Crick base pairing, which can alter the conformation of the tethered DNA from lying state to upright state. And these conformational alterations of the anchored DNA switches can effectively gate the transport of potassium ferricyanide onto the electrode interface. By continuously initiating the gates with DNA of different concentrations, we achieved the stepping gating of ion channels on a single nanoelectrode. Further, we demonstrated that the ion gating system on nanoelectrode showed excellent sensing performance. For example, the response kinetic was very fast with the signal saturation time of ~1 min, the reproducibility of the OFF/ON switch was robust enough to sustain for two cycles, and simultaneously, the specificity was high enough to distinguish complementary DNA and non-complementary DNA. When used for label-free DNA detection, the limit of detection can be as low as 10 pM. This study provides a promising avenue to achieve label free and real-time detection of multiple biomolecules.

1. Introduction

As a natural ion channel on biological membrane, transmembrane protein can gate the exchange of substances extracellularly and intracellularly upon extracellular stimuli by changing its conformation, such as the ligand binding-induced conformational alteration of receptor protein and voltage-sensitive transmembrane protein with variable structure (Unwin, 1993; Weyand and Iwata, 2010). Learning from nature, researchers have developed a variety of biomimetic response-to-stimulus ion channels, for example, using pH (Wang et al., 2017), voltage (Rant et al., 2007), temperature (Iftinca et al., 2006), ions (Wu et al., 2018) and light (Jia et al., 2016) as triggers to initiate the ionic gates for various applications including biosensing and sequencing. However, most of these previous ion channel gating systems are achieved by one-step initiation. And few reports explored the sensing property of the stepping gating system and used it for label-free detection.

Of particular interest, DNA or aptamers have been drawn extensive attentions by researchers due to its high controllability, high precisions, and high recognition capability (Abi et al., 2014; Bell et al., 2012; Plesa et al., 2014; Su et al., 2016; Wei et al., 2012; Song et al., 2019). Besides, DNA-based electrochemical sensors have been widely used for multi-molecular level detection including DNA (Abi et al., 2018; Barati Farimani et al., 2017; Das et al., 2016; Drummond et al., 2003; Fan et al., 2003; Xia et al., 2010), RNA (Ge et al., 2014; Lin et al., 2014; Mohamadi et al., 2015), proteins (Li et al., 2018) and small molecules (Adeel et al., 2019; Gorodetsky et al., 2008; Lin et al., 2016). However, most of the DNA electrochemical sensor is accomplished on gold macroelectrode interface. Sensing property of DNA probes modified on other sensing substrates should be further explored. Up to date, multiple conductive substrates have been developed during the past few years, such as elemental-doped mesoporous carbon nanosheets (Emran et al., 2018; Morgese et al., 2018) and nanoelectrodes (Wang et al., 2018). Attracted by its unique properties, such as high spatial resolution (Arbault et al., 2004; Clausmeyer and Schuhmann, 2016; Wu et al., 2005), fast mass-transfer rate (Heinze, 1993; Jung et al., 2018; Wipf and Wightman, 1988), low IR drop (Lambie et al., 2007),

* Corresponding authors.
E-mail addresses: xujiaqiang@shu.edu.cn (J. Xu), mlisinap@163.com (M. Li).

https://doi.org/10.1016/j.bios.2019.03.038
Received 23 January 2019; Received in revised form 10 March 2019; Accepted 17 March 2019
Available online 19 March 2019
0956-5663/

nanoelectrodes have been drawn extensive attention during the past few decades for achieving real-time monitoring of neurotransmitter secreted by neuron (Adams, 1990). It is worth mentioning that DNA anchored on such nanoelectrode interface showed prominent ion gating effect for small molecules, for example, potassium ferricyanide. And such prominent ion gating effect is indiscernible on macroelectrode. Based on the previous study (Liu et al., 2010), it is the unique nanoscale shape of the nanoelectrode that contributes to the ion gating effect.

Motivated by such ion gating effect of DNA anchored on nanoelectrode, here in this work, we constructed an ion gating system on gold nanoelectrode by anchoring single-stranded DNA (ssDNA) on the interface of it. The gold nanoelectrodes with uniform sizes can be obtained by using electrochemical etching technique. And the single-stranded DNA was anchored onto the interface of the gold nanoelectrode by the interaction between gold and thiol. Due to the fact that ssDNA is a flexible "soft" polymer and duplex DNA (dsDNA) is a "rigid" polymer (Bosco et al., 2012; Fan et al., 2003). The lying conformation of soft ssDNA capped the nanotip of the nanoelectrode tightly, with blocking the transport of potassium ferricyanide onto the interface of nanoelectrode. When triggered by the complementary DNA with different concentrations, the lying soft ssDNA on the nanoelectrode changes to rigid upright dsDNA gradually, which can initiate the ion gate switching on step-by-step, and simultaneously potassium ferricyanide can transport onto nanoelectrode and produce prominent redox current (Scheme 1). Interrogating the ion gating effect on nanoelectrode by electrochemical method, we demonstrated that the ion gating system on nanoelectrode possessed excellent sensing properties including fast response kinetics, high specificity and robust reproductivity. And using the ion gating effect, we could achieve the real-time detection of label-free DNA. This study provides a promising approach to accomplish real-time detection of label-free DNA or other biomolecules.

2. Materials and methods

2.1. Chemicals and Materials

All oligonucleotides were synthesized and purified by Sangon Biotech Co. Ltd (Shanghai, China). Hydrochloric acid (37%) was purchased from Suzhou Crystal Clear Chemical Co., Ltd. Tris (2-carboxyethyl)-phosphine hydrochloride (TCEP) and 6-mercaptohexanol (MCH) were purchased from Sigma-Aldrich (St. Louis, MO). AuNPs of 15 nm was purchased from Ted Pella, Inc. The Au microwires with the diameter of 0.25 mm (99.999% purity) were gained from China New Metal Materials Technology Co., Ltd. All other inorganic chemical reagents were purchased from Sinopharm Chemical reagent Co., Ltd and were used without further purification. All solutions were prepared with Milli-Q water (18 MΩ cm resistivity) from a Millipore system. DNA sequences of the oligonucleotides employed in this work (5′-3′) are as follows,

Capture probe: SH-ATGATGTTCGTTGTGTAGGATTTGC
Target DNA: GCAAATCCTACACAACGAACATCAT
Oligo 3: SH-TTTTTTTTTTGCAAATCCTACACAACGAACATCAT
Oligo 4: SH-GAAACCCTATGTATGCTCTTTTTTT
Noncomplementary DNA (Oligo 5): CACTCAATCCTCATCAATCTT ACTC

2.2. Apparatus

All the electrochemical experiments were carried out on a CHI 660E Electrochemical Workstation (CH Instruments Co., Ltd. Shanghai, China). Conventional three electrodes system where Ag/AgCl (3 M KCl) electrode as reference, Pt electrode as counter and gold nanoelectrode as work electrode, was used for all electrochemical detection. The electrochemical experiments were performed in the CHI 200B microcurrent amplifier and screen box. Scanning electron microscopy (SEM) images of the nanoelectrode tips were gained by the LEO 1530VP (Germany). Transmission electron microscopy (TEM) images of the nanoelectrode were obtained by the Tecnai G2 F20 S-TWIN (America).

2.3. Fabrication of single Au nanoelectrode

The gold nanoelectrodes was constructed by electrochemical etching in three steps (Ren et al., 2004; Wightman, 2006). Firstly, the Au wires with the diameter of 0.25 mm were ultrasonically rinsed with Milli-Q water, acetone and analytical grade ethanol, respectively. The 0.25 mm gold wires were stored in the ethanol/hydrochloric acid solution (1:1), and a DC potential of 2.2 V was applied between the Au wire and the Au ring (8 mm in diameter) counter electrode. Chronoamperometry (i-t) was used to record the current change in real-time during the gold etching process (tip 1). Secondly, the nanoelectrode were insulated with cathodic electrophoretic paint by electrodeposition in the DC potential of 30 V, 40 V and 80 V (tip 2) with the mass ratio of cathodic paint to ultrapure water 1:4. Thirdly, the electrode was dried in a baking oven under 105 °C for 30 min to solidify the paint decorated on the interface of nanoelectrode and expose the very nanotip of the nanoelectrode. The exposed nanotip of the nanoelectrode can be regulated by simply adjusting the electrodeposition times and the drying time (tip 3).

2.4. The fabrication of the self-assembled monolayer on nanoelectrodes

Firstly, the fresh-constructed nanoelectrode was incubated in the mixture containing 5 μM capture probe DNA and 500 nM MCH at room temperature for 7 h. Probe DNA and MCH were diluted with the buffer containing 10 mM Na_2HPO_4, 10 mM NaH_2PO_4, 20 mM $MgCl_2$, 1 M NaCl, (pH = 7.4). Then, the tip was rinsed with 10 mM PBS (10 mM Na_2HPO_4, 10 mM NaH_2PO_4, 100 mM NaCl, pH = 7.4), to decrease the nonspecific adsorption of DNA onto the interface of nanoelectrode.

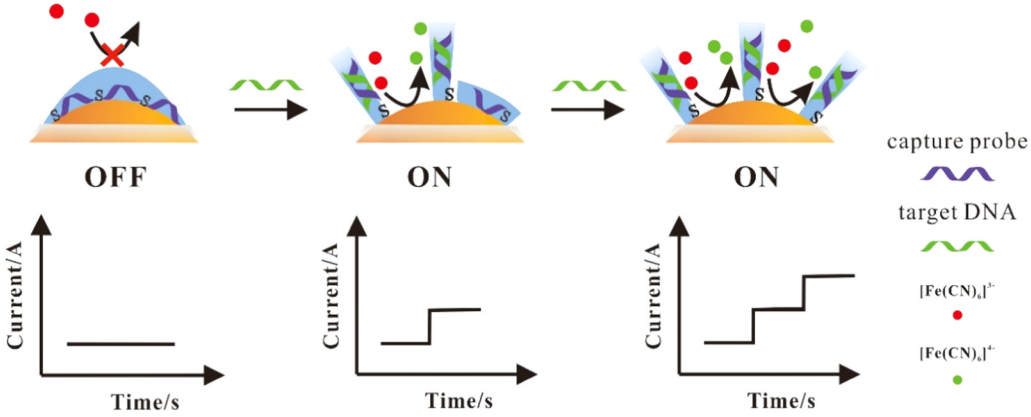

Scheme 1. Schematic illustration of stepping gating of potassium ferricyanide transferring onto gold nanoelectrode interface by the hybridization of DNA. The ssDNA layer in the nanoelectrode block electron transfer between the potassium ferricyanide ($Fe(CN)_6^{3-}$) and nanoelectrode remaining the ionic gate under off state. When hybridized with complementary strand, the lying surface-tethered DNA changed to rigid dsDNA with the ionic gate switch on.

2.5. Reaction between ssDNA-modified nanoelectrode and AuNPs-modified DNA

Thiol-modified DNA was firstly treated with TCEP (1:30 in concentration) under 95 ℃ for 10 min. Then the annealed DNA was mixed with 2.41 nM AuNPs (15 nm in diameter) under 4 ℃ for 7 h. 100 mM phosphate buffer (pH = 7.4) and 2 M NaCl were added into the AuNPs solution gradually to obtain DNA-AuNPs complex. After that ssDNA-modified nanoelectrode was immersed into the DNA-AuNPs complex at room temperature overnight.

3. Results and discussions

3.1. Characterization of gold nanoelectrode

The fabrication process of gold nanoelectrode was illustrated in Fig. 1A. Typical three-step method was used to construct gold nanoelectrodes with proper dimensions. To characterize the diameter of gold nanoelectrode, we first used scanning electron microscopy (SEM) to image the nanotip of nanoelectrode. The diameter of the gold nanoelectrode can be as thin as ~70 nm, indicating that the gold wires could be electrochemically etched as we expected (Fig. 1B). Then SEM and transmission electron microscopy (TEM) were used to characterize the insulation process of gold nanoelectrode. An approximate transparent paint layer was observed on the interface of nanoelectrode with the very nanotip exposed, which is similar to previous study (Liu et al., 2015). This result indicated that the nanoelectrode was insulated by cathodic electrophoretic paint electrochemically (Fig. 1C, Fig. S1A-C). Also, we characterized the gold nanoelectrode in 0.05 M H_2SO_4. The typical reductive peak of gold at ~0.85 V was observed from the cyclic voltammetry curve, indicating that the gold with nanotip was still exposed after insulation as we expected (Fig. S2). Besides, the prominently increased diameter after encapsulation with electrophoretic paint further suggested that the insulating layer was successfully deposited onto the interface of nanoelectrode (Fig. 1D, Fig. S1D).

Then we used cyclic voltammetry to characterize electrochemical property of nanoelectrode with different diameters in 10 mM $K_3Fe(CN)_6$ containing 0.5 M KCl. The uniform well-defined sigmoid-shaped voltammograms with different limiting currents illustrated that all the nanoelectrodes possessed excellent nonlinear diffusivity, which is the unique electrochemical property of micro/nanoelectrode. Supposing that the tip of the nanoelectrode is a hemispherical tip after insulation, the radius of the nanoelectrode can be calculated by the diffusion-limited steady-state current (Zoski and Mirkin, 2002):

$$i_0 = 2\pi nFDC_0r_0$$

where i_0 is the steady-state limiting current for the reduction of $K_3Fe(CN)_6$, n is the number of electron which was transferred per molecule (n = 1), C_0 is the concentration of potassium ferricyanide (10 mM), D is the diffusion coefficient of potassium ferricyanide ($D = 7.2 \times 10^{-6}$ cm^2 s^{-1}), F is the Faraday's constant ($F = 96485$ C mol^{-1}). Based on the equation and cyclic voltammetry, the radius of the nanoelectrodes increased along with the increased limiting current (from a to d, radius = 160 nm, 3.8 μm, 1.3 μm, and 2.5 μm, respectively). And subsequently, we selected nanoelectrodes with approximate uniform diameters (~70 nm) to evaluate the ion gating effect of ssDNA switch that anchored on the nanotip of nanoelectrode.

Next, we verified the stability of the encapsulated nanoelectrode by scanning cyclic voltammetry curves in 10 mM $K_3Fe(CN)_6$ containing 0.5 M KCl for multiple cycles. The approximate coincident curves for 70 scans indicated the admirable stability of the nanoelectrode (Fig. S3A). Also, we scanned the nanoelectrode in buffers with different pH. Although the curves obtained by different pH were discrepant, the curves under the same pH buffer coincided very well, suggesting that the nanoelectrode could maintain stability under certain condition (Fig. S3B). Additionally, the excellent overlays of the cyclic voltammetry curves

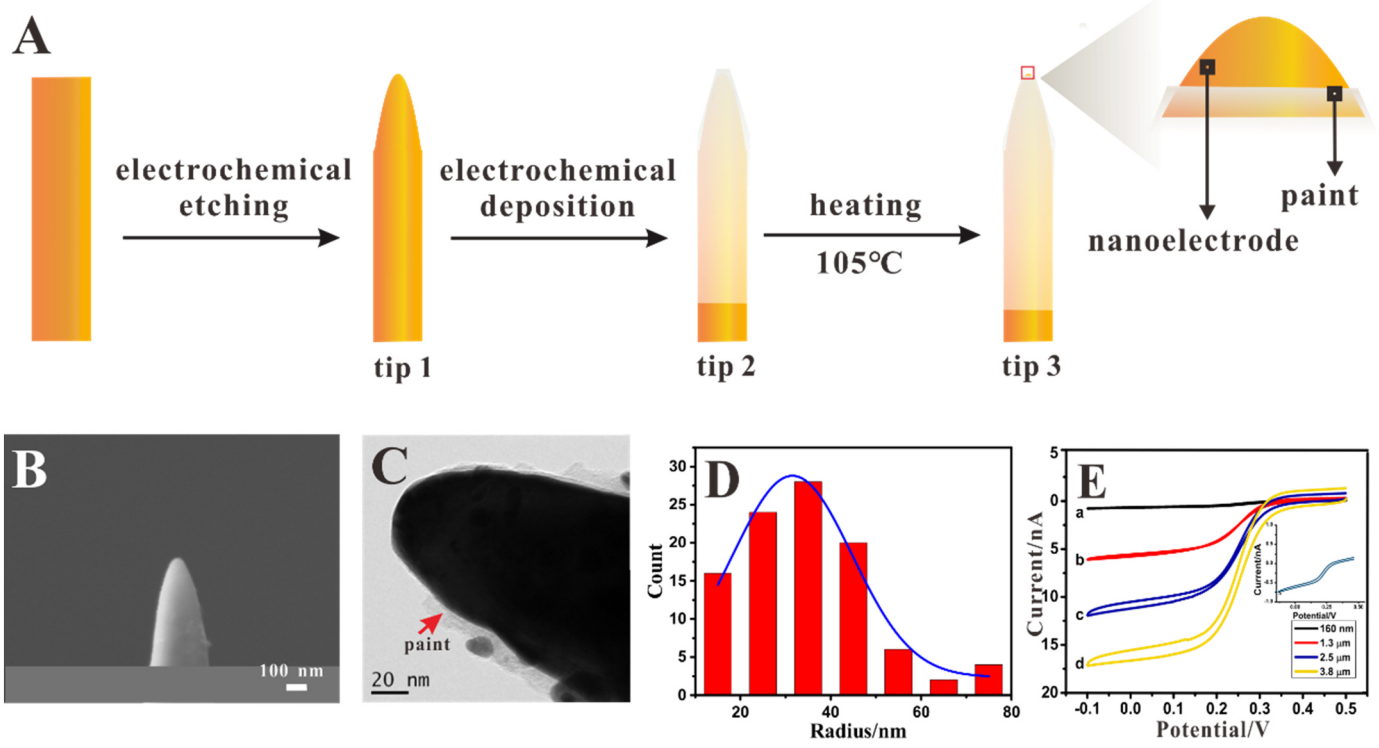

Fig. 1. The fabrication of gold nanoelectrode. A. Three steps (electrochemical etching, electrochemical deposition and heating) show the fabrication process of nanoelectrode. B. SEM characterization of the nanoelectrode. C. TEM characterization of the insulated paint electrochemically deposited onto the interface of gold nanoelectrode. D. Size distribution of gold nanoelectrodes without insulation. E. Cyclic voltammetry responses of nanoelectrode with different effective radius in 10 mM $K_3Fe(CN)_6$ containing 0.5 M KCl, scan rate: 50 mv/s.

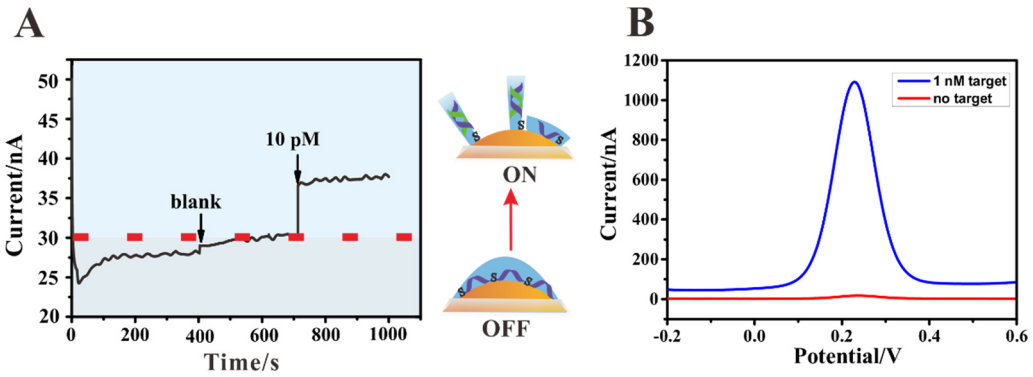

Fig. 2. Ion gating effect on nanoelectrode. A. Chronoamperometry response of ion channels triggered by 10 pM complementary DNA in 0.5 M $K_3Fe(CN)_6$, potential: 0.1 V vs. Ag/AgCl. B. Square wave voltammetry response of ion channels triggered by complementary DNA of 1 nM.

scanned with different buffers further indicated the robust stability of the nanoelectrode (Fig. S3C).

3.2. Stepping gating of ion channels on nanoelectrode

To evaluate the ion gating effect of ssDNA anchored on gold nanoelectrode. Firstly, we recorded the real-time gating current response of 0.5 M $K_3Fe(CN)_6$ by chronoamperometry. The rapid increase of steady-state current after the introduction of 10 pM complementary DNA initiator indicated that the gate was switched on immediately. And the switching on process was accomplished by the lying conformation of ssDNA changing to upright orientation because of the Watson-Crick base pairing (Fig. 2A), which simultaneously increased the probabilities that $K_3Fe(CN)_6$ contacted with the nanoelectrode interface. Besides, the ion gating effect was also verified by electrochemical square wave voltammetry (SWV). After the initiation by complementary DNA, we observed prominent increase of the current peak at the potential of ~0.25 V (Fig. 2B), indicating that more $K_3Fe(CN)_6$ molecules contacted with the nanoelectrode with the ion gates switching on. Then the switching on mechanism was further verified by visually confirming the hybridization between ssDNA and complementary DNA. To demonstrate the hybridization, we modified the complementary DNA by AuNPs with the diameter of 15 nm. Characterized by SEM imaging, homogeneous distribution of AuNPs was observed on the interface of nanoelectrode when initiated by complementary DNA (Fig. S4A). As a contrast, negligible AuNPs was observed on the interface of nanoelectrode when triggered by noncomplementary DNA. These results suggested that the ion gating switches were initiated by the hybridization between DNAs (Fig. S4B).

Next, we used cyclic voltammetry to verify the stepping regulation of the gate. To verify the stepping gating effect, we triggered the ion channels that anchored on the same single nanoelectrode by introducing DNA of gradually increased concentrations. The gradient increased limiting currents when triggered by complementary DNA of increased concentrations suggested that the ion gates were switched on step by step (Fig. 3B). Similarly, when interrogated by SWV, gradient increase of the peak current at the potential of ~0.25 V further indicated the stepping gating capability of ion channels on nanoelectrode (Fig. 3C). Then, we evaluated the response kinetics of the ion gating system. Defining the signal steady-state time is the ion channel response time, we found that the switching kinetics of the ion channel could be as fast as ~1 min. This result indicated that the ion channel could be triggered rapidly and in real-time due to the fast mass-transfer property of the nanoelectrode (Fig. 3D).

3.3. Label-free DNA detection by ion gating system

To achieve the label-free DNA detection, we first verified the specificity of the ion gating system by introducing random DNA sequences (Oligo 5). When triggering the ion channels by complementary DNA strands of 10 pM, we observed approximated ~350% signal increase of the ion gating system on nanoelectrode. However, negligible signal change was obtained when the ion channels were triggered by the noncomplementary DNA of 10 nM, the concentration of which was 1000-fold higher than that of complementary DNA. And such ignorable signal change was approximately equivalent to the background signal variation. These results indicated that the gating system on nanoelectrode showed high specificity to exogenous stimulation (Fig. 4A). Further, the specificity of the ion gating system was confirmed by the hybridization between ssDNA and AuNPs-modified DNA. The number of AuNPs on nanoelectrode that triggered by AuNPs-modified complementary DNA was prominent more than that triggered by noncomplementary DNA. These results further illustrated the high specificity of the ion gating system (Fig. S4).

Then we verified the regeneration capability of the ion gating system. Using the property of DNA untwisting when challenged with low-salt buffer or Milli-Q water, we recovered the ion gating system by simply immersing the ion channel-contained nanoelectrode that under on states in Milli-Q water overnight. The approximate equivalent signal variation (~573% signal increase for the first cycle and ~548% signal increase for the second cycle) during the two OFF/ON switching cycles indicated that the ion gating system was quite stable with excellent reproducibility (Fig. 4B).

Having confirmed the excellent sensing property of the ion gating system on nanoelectrode, such as fast response kinetics, high specificity and stable reproducibility, we finally used the ion gating system to detect label-free DNA. Using SWV to interrogate the determination, we found that the peak current increased along with the increased concentration of the label-free DNA. And the signal obtained saturation until the all the ionic gates on the interface of nanoelectrode were switched on with the maximum concentration of label-free DNA of 1 nM (Fig. 4C). And the limit of detection for label-free DNA could be as low as 10 pM which is lower than previous report, the limit of detection of which was 1 nM (Liu et al., 2010), achieving the excellent label-free DNA sensing examination.

4. Conclusions

In summary, we demonstrated a stepping ion gating system on a single gold nanoelectrode by anchoring ssDNA on the very nanotip of the nanoelectrode. By continuously triggering the ion channels with different concentration DNA, we achieved the stepping gating of the ion channels on the same single nanoelectrode. Furthermore, the ion gating system constructed on nanoelectrode showed fast response kinetics with the response time less than 1 min. Also, simultaneously, the reproducibility was robust enough to sustain for two cyclic OFF/ON switches. Besides, the specificity of the ion switch was very high which could distinguish complementary DNA and noncomplementary DNA. Using the ion gating system on nanoelectrode with excellent sensing property, we achieved the label-free DNA detection with the limit of detection of 10 pM. This study provides a prospective approach for achieving label-free detection for multiplex targets including small molecules and proteins by changing the tethered DNA to an aptamer.

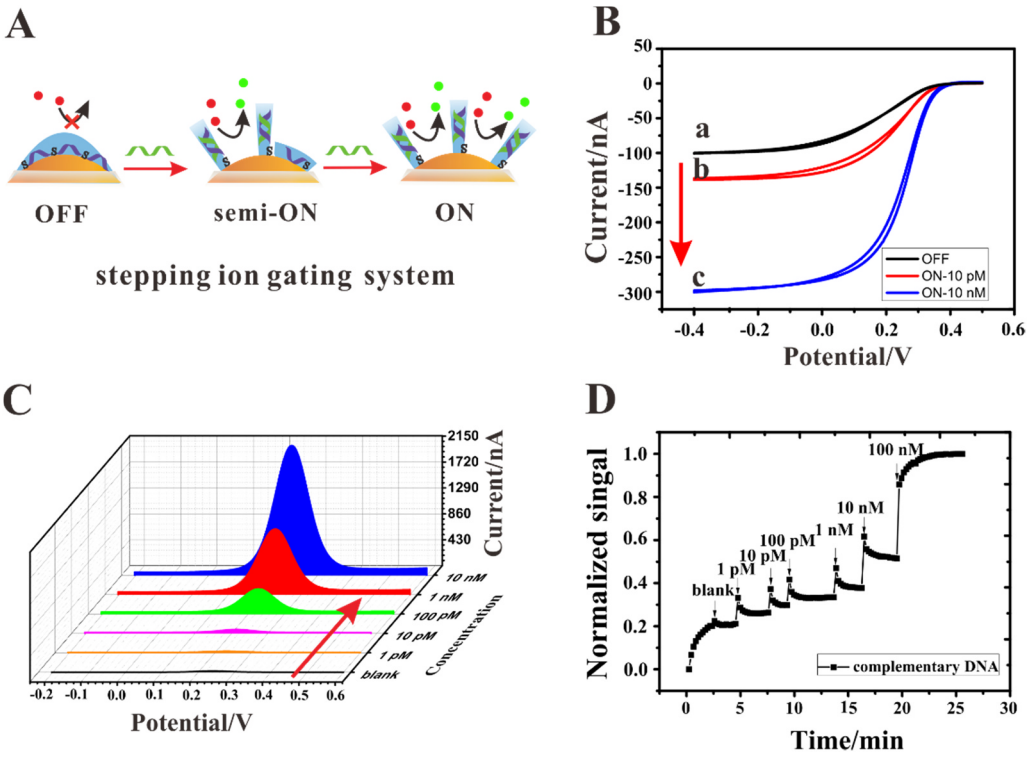

Fig. 3. Stepping gating of the ion channels on nanoelectrode. A. Stepping gating of ion gate triggered by complementary DNA. B. Cyclic voltammetry response of ion channels triggered by complementary DNA of different concentrations. C. A typical square wave voltammetry plot of ion channels triggered by the successive addition of target DNA (0 pM, 1 pM, 10 pM, 100 pM, 1000 pM, 10 nM), with frequency of 25 Hz. D. Real time current response of ion channels triggered by the successive addition of target DNA (0 pM, 1 pM, 10 pM, 100 pM, 1000 pM, 10 nM), with the signal saturation time of ~1 min.

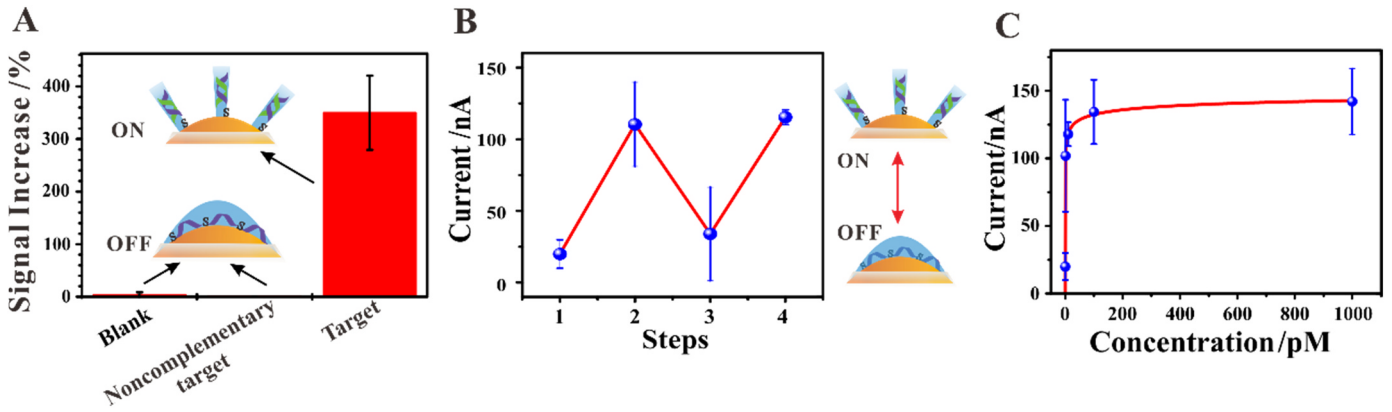

Fig. 4. A. Specificity characterization of the ion gating system on nanoelectrode using SWV by introducing of noncomplementary DNA. The concentration of complementary DNA and noncomplementary DNA were 10 pM and 10 nM respectively. B. The regeneration capability of the ion gating system for two cycles. C. Titration curve for label-free DNA detection with the limit of detection of 10 pM.

CRediT authorship contribution statement

Haipei Zhao: Conceptualization, Data curation, Investigation, Methodology. **Dekai Ye:** Conceptualization, Data curation, Investigation, Methodology. **Xiuhai Mao:** Conceptualization, Data curation, Investigation, Methodology. **Fan Li:** Conceptualization, Data curation, Investigation, Methodology. **Jiaqiang Xu:** Supervision, Validation. **Min Li:** Writing - original draft, Writing - review & editing. **Xiaolei Zuo:** Funding acquisition, Project administration, Resources.

Acknowledgments

This work was supported by Shanghai Municipal Education Commission-Gaofeng Clinical Medicine Grant Support (20171913).

Conflicts of interest

The authors declare no competing financial interest.

Declaration of interests

None.

Credit authors statement

The authors' individual contributions are as follows:

Haipei Zhao, Dekai Ye, Xiuhai Mao, and Fan Li are responsible for Conceptualization; Data curation; Investigation; Methodology.

Jiaqiang Xu is responsible for Supervision and Validation.

Min Li is responsible for Roles/Writing - original draft; Writing - review & editing

Xiaolei Zuo is responsible for Funding acquisition; Project

administration and Resources;

Appendix A. Supporting information

Supplementary data associated with this article can be found in the online version at doi:10.1016/j.bios.2019.03.038.

References

Abi, A., Lin, M., Pei, H., Fan, C., Ferapontova, E.E., Zuo, X., 2014. ACS Appl. Mater. Interfaces 6, 8928–8931.
Abi, A., Mohammadpour, Z., Zuo, X., Safavi, A., 2018. Biosens. Bioelectron. 102, 479–489.
Adams, R.N., 1990. Prog. Neurobiol. 35, 297–311.
Adeel, M., Rahman, M.M., Lee, J.-J., 2019. Biosens. Bioelectron. 126, 143–150.
Arbault, S., Sojic, N., Bruce, D., Amatore, C., Sarasin, A., Vuillaume, M., 2004. Carcinogenesis 25, 509–515.
Barati Farimani, A., Dibaeinia, P., Aluru, N.R., 2017. ACS Appl. Mater. Interfaces 9, 92–100.
Bell, N.A., Engst, C.R., Ablay, M., Divitini, G., Ducati, C., Liedl, T., Keyser, U.F., 2012. Nano Lett. 12, 512–517.
Bosco, A., Bano, F., Parisse, P., Casalis, L., DeSimone, A., Micheletti, C., 2012. Nanoscale 4, 1734–1741.
Clausmeyer, J., Schuhmann, W., 2016. Trends Anal. Chem. 79, 46–59.
Das, J., Ivanov, I., Sargent, E.H., Kelley, S.O., 2016. J. Am. Chem. Soc. 138, 11009–11016.
Drummond, T.G., Hill, M.G., Barton, J.K., 2003. Nat. Biotechnol. 21, 1192–1199.
Emran, M.Y., Shenashen, M.A., Morita, H., El-Safty, S.A., 2018. Biosens. Bioelectron. 109, 237–245.
Fan, C., Plaxco, K.W., Heeger, A.J., 2003. Proc. Natl. Acad. Sci. USA 100, 9134–9137.
Ge, Z., Lin, M., Wang, P., Pei, H., Yan, J., Shi, J., Huang, Q., He, D., Fan, C., Zuo, X., 2014. Anal. Chem. 86, 2124–2130.
Gorodetsky, A.A., Ebrahim, A., Barton, J.K., 2008. J. Am. Chem. Soc. 130, 2924–2925.
Heinze, J., 1993. Angew. Chem. Int. Ed. 32, 1268–1288.
Iftinca, M., McKay, B.E., Snutch, T.P., McRory, J.E., Turner, R.W., Zamponi, G.W., 2006. Neuroscience 142, 1031–1042.
Jia, C., Migliore, A., Xin, N., Huang, S., Wang, J., Yang, Q., Wang, S., Chen, H., Wang, D., Feng, B., Liu, Z., Zhang, G., Qu, D.-H., Tian, H., Ratner, M.A., Xu, H.Q., Nitzan, A., Guo, X., 2016. Science 352, 1443–1445.
Jung, S.W., Kim, H.S., Cho, A.E., Kim, Y.-H., 2018. ACS Appl. Mater. Interfaces 10, 18227–18236.
Lambie, B.A., Brennan, C., Olofsson, J., Orwar, O., Weber, S.G., 2007. Anal. Chem. 79, 3771–3778.
Li, M., Guo, X., Li, H., Zuo, X., Hao, R., Song, H., Ali, A., Ge, Z., Li, J., Li, Q., Song, S., Li, S., Shao, N., Fan, C., Wang, L., 2018. ACS Appl. Mater. Interfaces 10, 341–349.
Lin, M., Song, P., Zhou, G., Zuo, X., Aldalbahi, A., Lou, X., Shi, J., Fan, C., 2016. Nat. Protoc. 11, 1244–1263.
Lin, M., Wen, Y., Li, L., Pei, H., Liu, G., Song, H., Zuo, X., Fan, C., Huang, Q., 2014. Anal. Chem. 86, 2285–2288.
Liu, G., Sun, C., Li, D., Song, S., Mao, B., Fan, C., Tian, Z., 2010. Adv. Mater. 22, 2148–2150.
Liu, Y., Li, M., Zhang, F., Zhu, A., Shi, G., 2015. Anal. Chem. 87, 5531–5538.
Mohamadi, R.M., Ivanov, I., Stojcic, J., Nam, R.K., Sargent, E.H., Kelley, S.O., 2015. Anal. Chem. 87, 6258–6264.
Morgese, G., Benetti, E.M., Zenobi-Wong, M., 2018. Adv. Healthc. Mater. 7, 1701459.
Plesa, C., Ananth, A.N., Linko, V., Gülcher, C., Katan, A.J., Dietz, H., Dekker, C., 2014. ACS Nano 8, 35–43.
Rant, U., Arinaga, K., Scherer, S., Pringsheim, E., Fujita, S., Yokoyama, N., Tornow, M., Abstreiter, G., 2007. Proc. Natl. Acad. Sci. USA 104, 17364–17369.
Ren, B., Picardi, G., Pettinger, B., 2004. Rev. Sci. Instrum. 75, 837–841.
Song, Y., Shi, Y., Huang, M., Wang, W., Wang, Y., Cheng, J., Lei, Z., Zhu, Z., Yang, C., 2019. Angew. Chem. Int. Ed. 58, 2236–2240.
Su, S., Sun, H., Cao, W., Chao, J., Peng, H., Zuo, X., Yuwen, L., Fan, C., Wang, L., 2016. ACS Appl. Mater. Interfaces 8, 6826–6833.
Unwin, N., 1993. Cell 72, 31–41.
Wang, D., Xiao, X., Xu, S., Liu, Y., Li, Y., 2018. Biosens. Bioelectron. 99, 431–437.
Wang, J., Fang, R., Hou, J., Zhang, H., Tian, Y., Wang, H., Jiang, L., 2017. ACS Nano 11, 3022–3029.
Wei, R., Martin, T.G., Rant, U., Dietz, H., 2012. Angew. Chem. Int. Ed. 51, 4864–4867.
Weyand, S., Iwata, S., 2010. Science 329, 151–152.
Wightman, R.M., 2006. Science 311, 1570–1574.
Wipf, D.O., Wightman, R.M., 1988. Anal. Chem. 60, 2460–2464.
Wu, W.-Z., Huang, W.-H., Wang, W., Wang, Z.-L., Cheng, J.-K., Xu, T., Zhang, R.-Y., Chen, Y., Liu, J., 2005. J. Am. Chem. Soc. 127, 8914–8915.
Wu, Y., Wang, D., Willner, I., Tian, Y., Jiang, L., 2018. Angew. Chem. Int. Ed. 57, 7790–7794.
Xia, F., Zuo, X., Yang, R., Xiao, Y., Kang, D., Vallée-Bélisle, A., Gong, X., Yuen, J.D., Hsu, B.B.Y., Heeger, A.J., Plaxco, K.W., 2010. Proc. Natl. Acad. Sci. USA 107, 10837–10841.
Zoski, C.G., Mirkin, M.V., 2002. Anal. Chem. 74, 1986–1992.